Influence of irrigation on root zone storage capacity estimation

Fransje van Oorschot[1,2], Ruud van der Ent[1], Andrea Alessandri[2], and Markus Hrachowitz[1]

[1]Department of Water Management, Faculty of Civil Engineering and Geosciences, Delft University of Technology, Delft, The Netherlands

[2]Institute of Atmospheric Sciences and Climate, National Research Council of Italy (CNR-ISAC), Bologna, Italy

Correspondence: Fransje van Oorschot (f.vanoorschot@tudelft.nl)

Abstract. Vegetation plays a crucial role in regulating the water cycle through transpiration, which is the water flux from the subsurface to the atmosphere via vegetation roots. The amount and timing of transpiration is controlled by the interplay of seasonal energy and water supply. The latter strongly depends on the size of the root zone storage capacity (S_r) which represents the maximum accessible volume of water that vegetation can use for transpiration. S_r is primarily influenced by hydro-climatic conditions as vegetation optimizes its root system in a way it can guarantee water uptake and overcome dry periods. S_r estimates are commonly derived from root zone water deficits that result from the phase shift between the seasonal signals of root zone water inflow (i.e., precipitation) and outflow (i.e., evaporation). In irrigated croplands, irrigation water serves as an additional input into the root zone. However, this aspect has been ignored in many studies, and the extent to which irrigation influences S_r estimates was never comprehensively quantified. In this study, our objective is to quantify the influence of irrigation on S_r and identify the regional differences therein. To this aim, we integrated two irrigation methods, based on irrigation water use and irrigated area fractions, respectively, into the S_r estimation. We evaluated the effects in comparison to S_r estimates that do not consider irrigation for a sample of 4856 catchments globally with varying degrees of irrigation activities. Our results show that S_r consistently decreased when considering irrigation with a larger effect in catchments with a larger irrigated area. For catchments with an irrigated area fraction exceeding 10 %, the median decrease of S_r was 19 mm and 23 mm for the two methods, corresponding to 12 % and 15 %, respectively. S_r decreased the most for catchments in tropical climates. However, the relative decrease was the largest in catchments in temperate climates. Our results demonstrate, for the first time, that irrigation has a considerable influence on S_r estimates over irrigated croplands. This effect is as strong as the effects of snow melt that were previously documented in catchments that have a considerable amount of precipitation falling as snow.

1 Introduction

Vegetation strongly influences the water cycle as it controls the partitioning of precipitation into discharge and evaporation by mediating soil evaporation, interception evaporation and transpiration (Milly, 1994). Transpiration is defined as the water

transport from the subsurface back to the atmosphere via the roots of vegetation, and is, on average, the largest terrestrial water flux globally (Schlesinger and Jasechko, 2014). The amount and timing of vegetation transpiration at catchment scales is largely controlled by the interplay between seasonal energy and water availability signals (Gentine et al., 2012). At individual plant scale, plants regulate transpiration also by root biomass adjustments, anatomical alterations, and physiological acclimation (e.g. Brunner et al., 2015), depending on the vegetation species (Zhang et al., 2020). However, at the ecosystem scale, which represents the collective of individual plants, the subsurface water removal by transpiration is regulated by the liquid water input and by the available subsurface water buffer. This water buffer, the root zone storage capacity (S_r), is defined as the maximum volume per unit square of subsurface moisture that is accessible to roots of vegetation for uptake (Gao et al., 2014). S_r is an essential property of hydrological systems – and parameter in land surface models and hydrological models – regulating terrestrial water, carbon and energy balances at all scales from plot to global (Seneviratne et al., 2010; Wang and Dickinson, 2012; Dralle et al., 2020a; Singh et al., 2022). Increasing evidence suggests that the extent of vegetation root systems, and consequently the magnitude of S_r, is primarily controlled by climate conditions (Kleidon and Heimann, 1998; Gao et al., 2014; De Boer-Euser et al., 2016; Kuppel et al., 2017). More specifically, the results of many studies suggest that the extent of root systems is a manifestation of vegetation (i.e., the collective of all individual plants within a specified spatial domain) having efficiently adapted to past hydro-climatic conditions. In other words, individual plants within an ecosystem have survived in competition with other plants as they found a more efficient (or optimal) balance between above-ground and below-ground resource allocation (Kleidon and Heimann, 1998; Collins and Bras, 2007; Guswa, 2008; Sivandran and Bras, 2013; Fan et al., 2017; Singh et al., 2020). Direct observations of S_r at scales larger than plot scale do not exist and, therefore, several indirect methods have been developed to estimate S_r from other observable ecosystem properties considering optimality principles (Kleidon, 2004; Gao et al., 2014; Speich et al., 2018; Dralle et al., 2020a).

One of these methods is the memory method, a term coined by Van Oorschot et al. (2021), but also referred to as water balance method (Nijzink et al., 2016; Hrachowitz et al., 2021) or mass curve technique (Gao et al., 2014; Zhao et al., 2016). This method allows to estimate S_r based on root zone water deficits arising from the phase shift between the seasonal signals of precipitation and evaporation, here defined as the total of transpiration, soil evaporation, and interception evaporation, following the terminology proposed by Savenije (2004) and Miralles et al. (2020). This approach is based on evidence that root systems of present-day vegetation are a legacy that reflects the memory of past water deficits during dry spells. Vegetation has efficiently adapted the extent of its root system to past water deficits with a specific memory (i.e. the dry spell return period) to guarantee continuous access to water to satisfy canopy water demand, but no more than that (Savenije and Hrachowitz, 2017). Numerous studies have successfully demonstrated the potential of the memory method to provide estimates of climate controlled S_r for river catchments based on discharge data (Gao et al., 2014; De Boer-Euser et al., 2016; Van Oorschot et al., 2021), as well as on larger scales based on remotely sensed estimates of evaporation (Wang-Erlandsson et al., 2016; Singh et al., 2020; McCormick et al., 2021; Stocker et al., 2023). In addition, the method proved valuable to track the temporal evolution of S_r due to changing hydro-climatic conditions (Bouaziz et al., 2022) and human interventions, such as forest management (Nijzink et al., 2016; Hrachowitz et al., 2021).

It is important to note that the memory method is based on liquid water input to the root zone. As such, solid phase precipitation and storage as transient, seasonal or perennial snow packs introduces time lags between the moment of precipitation and the release of liquid water (i.e., melt water) into the sub-surface. These time lags can lead to considerable temporal shifts in liquid water supply, thereby affecting the development of seasonal water deficits and the associated magnitudes of S_{r}. Various models with different levels of complexity have previously been integrated into the memory method to account for the time lags due to snow accumulation and melt dynamics (de Boer-Euser et al., 2018; Dralle et al., 2021; Stocker et al., 2023). Dralle et al. (2021) have recently shown that explicitly accounting for snow accumulation and associated time lags in melt water release in the memory method does generally lead to lower values of S_{r} in regions where significant fraction of precipitation occurs in the form of snow.

Irrigation similarly affects the timing of water input to the soil. Besides its effect on timing, irrigation during the growing season leads to input of additional water next to precipitation that otherwise would not be accessible for roots and thus not be available for vegetation uptake. Irrigation thereby also affects the magnitude of water input and actively shapes the root development of crops. Irrigation leads to shallower roots and higher root densities in the upper soil compared to non-irrigated vegetation, as it reduces the need for resource allocation for root growth, and instead allows increased resource allocation for above-surface growth (Klepper, 1991; Engels et al., 1994; Bakker et al., 2009; Maan et al., 2023). The strength of this signal is variable and depends on the irrigation method applied (Lv et al., 2010; Jha et al., 2017; Wang et al., 2020). Currently, approximately 20 % of global croplands are irrigated (FAO, 2022) and with the increasing demand for crop production, irrigation requirements are expected to increase in the future (Alexandratos and Bruinsma, 2012). In spite of some exceptions (e.g. Roodari et al. (2021)), irrigation is rarely systematically represented in hydrological and biogeophysical models (McDermid et al., 2023), mostly due to a lack of sufficient data (e.g., Meier et al. (2018)). This also holds for the memory method, as most studies using the memory method for S_{r} estimation did not account for irrigation, which likely led to an overestimation of S_{r} in irrigated areas (Gao et al., 2014; De Boer-Euser et al., 2016; Stocker et al., 2023). To our knowledge, only Wang-Erlandsson et al. (2016) explicitly accounted for irrigation when estimating S_{r} by adding irrigation estimates simulated by the LPJmL dynamic global vegetation model to the precipitation input (Jägermeyr et al., 2015). However, it remains unknown to which extent irrigation influences the magnitudes of S_{r} estimates and in which regions globally it is most relevant to take into account.

Our objective here is to quantify the influence of irrigation on the root zone storage capacity estimated with the memory method and to identify the regional differences therein. We do so by using a sample of 4856 catchments globally with varying degrees of irrigation activities. Specifically, we test the hypothesis that irrigation considerably reduces root zone storage capacities S_{r} and therefore needs to be accounted for in the estimation of S_{r}. To this aim, we introduce two methods that represent irrigation based on catchment water balances to the memory method using irrigation data from two different sources. The first method explicitly uses estimates of irrigation water use from Zhang et al. (2022) in the S_{r} calculation with the memory method. The second method is a simpler parameterization based on the irrigated area fraction (Siebert et al., 2015b).

2 Methods

2.1 Data

For this study we used station based discharge (Q) data from the following sources: the Global Streamflow Indices and Metadata Archive (GSIM) (Do et al., 2018; Gudmundsson et al., 2018), the Australian edition of the Catchment Attributes and Meteorology for Large-sample Studies (CAMELS-AUS) dataset (Fowler et al., 2021), the LArge-SaMple DAta for Hydrology and Environmental Sciences for Central Europe (LamaH-CE) (Klingler et al., 2021) and the Italian Hydrological Portal (Lendvai, 2020). We used annual mean discharge ($\overline{Q}$) for the catchment specific available time period. For the period 1981-2010, we obtained catchment average daily precipitation (P) and daily mean temperature (T_a) from the Global Soil Wetness Project Phase 3 (GSWP3) (Dirmeyer et al., 2006) and daily potential evaporation (E_p) from the Global Land Evaporation Amsterdam Model version 3.5a (GLEAMv3.5a), which is based on the Priestley-Taylor approach (Martens et al., 2017; Miralles et al., 2011). We selected 4856 catchments based on the following criteria: (1) at least 10 years of Q data during the 1981–2010 period; (2) catchment area < $10000\,\mathrm{km}^2$ to limit the heterogeneity within catchments; (3) annual mean discharge ($\overline{Q}$) smaller than annual mean precipitation ($\overline{P}$) for the specific catchment.

For each catchment we obtained irrigation estimates from two different data sources. Firstly, we used the average irrigated area fraction I_a (-), which is the areal fraction of land equipped with infrastructure for irrigation. I_a was obtained from the "AEI_HYDE_FINAL_IR" dataset developed by Siebert et al. (2015b), which is representative for the irrigation extent in the year 2005 (Fig. 1a). This dataset was based on sub-national irrigation statistics and the History Database of the Global Environment (HYDE) version 3.1 land use data (Klein Goldewijk et al., 2011; Siebert et al., 2015b). Secondly, we used estimates of annual mean irrigation water use representative for the 2011-2018 period ($\overline{I_\mathrm{w}}$ ($\mathrm{mm\,year}^{-1}$)) from Zhang et al. (2022), who developed an algorithm to estimate irrigation from multiple satellite-based products and the Priestley-Taylor Jet Propulsion Laboratory (PT-JPL) model (Fig. 1b).

To identify the effects of irrigation for different regions, we used the Köppen-Geiger climate classes as a climate indicator. We selected for each catchment the predominant Köppen-Geiger climate class based on a global map at a $1\,\mathrm{km}$ resolution representing the 1980-2016 period (Beck et al., 2018a). The gridded data products for P, E_p, I_a and $\overline{I_\mathrm{w}}$ were converted to catchment estimates using area weighted averages of the grid cells that lie for more than $50\,\%$ inside the catchment. Before area weighting, the gridded products were resampled to a spatial resolution of 0.05°using nearest neighbour interpolation. This way, all gridded products were treated similarly and problems with small catchments with no matching grid cells were avoided.

2.2 Memory method with irrigation methods

Figure 2a shows a conceptualization of the memory method based on four storage components (mm): interception storage S_i, snow storage S_sn, "surplus" storage S_s, and storage deficit S_d. S_d is initially conceptualized as an infinite deficit storage

120 volume and its temporal evolution can be described by:

$$S_{\mathrm{d}}(t) = \int_{t_0}^{\tau} (P_{\mathrm{e}} - E_{\mathrm{t}} + I - P_{\mathrm{s}}) \mathrm{d}t \tag{1}$$

where P_{e} represents effective precipitation ($\mathrm{mm\,day^{-1}}$), E_{t} is transpiration ($\mathrm{mm\,day^{-1}}$), I is irrigation ($\mathrm{mm\,day^{-1}}$), and P_{s} is surplus precipitation ($\mathrm{mm\,day^{-1}}$) (Fig. 2a). In Eq. (1) t_0 corresponds to the first day of the first hydrological year and τ to the daily time steps ending on the last day of the last hydrological year. Our hydrological year starts the first day of the month
125 after the wettest month, which is defined as the month with on average the largest positive difference between monthly mean P and E_{p}. At t_0, the starting point of the analysis, S_{d}=0. In Eq. (1), P_{e} ($\mathrm{mm\,day^{-1}}$) is calculated from the water balance of the interception storage S_{i} (Fig. 2a), and E_{t} ($\mathrm{mm\,day^{-1}}$) is described as a fraction of daily potential evaporation E_{p} ($\mathrm{mm\,day^{-1}}$) based on the catchment water balance. We used a simple snow model based on the degree-day method (e.g. Bergstrom, 1975; Gao et al., 2017) to account for the delay in liquid water input to the soil by describing liquid precipitation (P_{l} ($\mathrm{mm\,day^{-1}}$)),
130 precipitation falling as snow (P_{sn} ($\mathrm{mm\,day^{-1}}$)), and snow melt (P_{m} ($\mathrm{mm\,day^{-1}}$)). The equations for the interception storage, snow storage, and transpiration calculation are described in Appendix A.

Surplus precipitation P_{s} ($\mathrm{mm\,day^{-1}}$) in Eq. (1) is described by Eq. (2), in which we used the following notation for the sum of the fluxes between two time steps: $F_t = \int_{t-1}^{t} F \mathrm{d}t$, where F is either P_{e}, E_{t}, I or P_{s}. Thus $P_{\mathrm{s},t}$ is described by:

$$P_{\mathrm{s},t} = \max(0, S_{\mathrm{d}} + P_{\mathrm{e},t} - E_{\mathrm{t},t} + I_t), \tag{2}$$

135 with S_{d} and I_t approaching zero during periods of abundant precipitation, and thus it then holds that $P_{\mathrm{s},t} \approx P_{\mathrm{e},t} - E_{\mathrm{t},t}$.

For the computation of applied irrigation I we split the timeseries into surplus and deficit periods (Fig. 2b). For each hydrological year, we defined one deficit period, which is the longest deficit period with the largest S_{d} in the hydrological year. Surplus periods were defined as the periods in between the deficit periods. For each surplus period, the surplus precipitation P_{s} (Eq. (2)) accumulates in the surplus store S_{s}:

$$S_{\mathrm{s}}(t) = \max(0, \int_{t_{s0}}^{t_{s1}} (P_{\mathrm{s}} - I) \mathrm{d}t) \tag{3}$$

with t_{s0} the first day of the surplus period and t_{s1} the last day of the surplus period (Fig. 2b). S_{s} does not have a maximum storage capacity, but it is reset to zero each year, after each deficit period. This storage conceptualizes any water buffers that can be used for irrigation in the consecutive deficit period and may encompass ditches, lakes and aquifers. This method assumes that irrigated water only originates from water inside the catchment boundaries and that it is sustainably extracted so that the
145 long term water balance is closed. During a deficit period, the fraction of S_{s} that is used for irrigation is defined by irrigation factor f (-), which determines how much of the surplus water stored during the surplus period is used for irrigation during the consecutive deficit period. f represents both the water evaporated or discharged during the irrigation process before recharging the soil, and the spatial extent of the irrigation. It is assumed that daily irrigation I is equally distributed over the deficit period (Fig. 2b), so that I ($\mathrm{mm\,day^{-1}}$) is defined as:

$$I(t) = \frac{f S_{\mathrm{s}}(t_{s1})}{\Delta t_{\mathrm{d}}} \tag{4}$$

with Δt_{d} the length of the deficit period ($t_{d1} - t_{d0}$) in days (Fig. 2b). Based on the two irrigation data sources used (Sect. 2.1), we have here developed two methods to estimate f in Eq. (4):

1. Irrigation Water Use method (IWU)

   $f_{d,\mathrm{IWU}}$ (-) is defined for each deficit period d for each catchment by:

   $$f_{d,\mathrm{IWU}} = \max(1, \frac{\overline{I_{\mathrm{w}}}\mathrm{d}t}{S_{\mathrm{s}}(t_{s,1})}), \text{ so that } I(t) = \frac{\overline{I_{\mathrm{w}}}\mathrm{d}t}{\Delta t_{\mathrm{d}}} \text{if sufficient water is available in } S_{\mathrm{s}}, \quad (5)$$

   with $\overline{I_{\mathrm{w}}}$ ($\mathrm{mm\,year^{-1}}$) the catchment annual mean irrigation water use, $\mathrm{d}t = 1\,\mathrm{year}$, and $S_{\mathrm{s}}(t_{s,1})$ (mm) the surplus storage at the end of the surplus storage accumulation period, i.e. the amount of water stored in S_{s} at the start of the deficit period. In this method, $f_{d,\mathrm{IWU}}$ is different for each deficit period d, as S_{s} also varies. For each catchment, f_{IWU} is defined as the average $f_{d,\mathrm{IWU}}$.

2. Irrigated Area Fraction method (IAF)

   f_{IAF} (-) is temporally non-varying, and is defined for each catchment by:

   $$f_{\mathrm{IAF}} = \beta I_{\mathrm{a}} \quad (6)$$

   with I_{a} (-) the catchment irrigated area fraction and β (-) a correction factor that is constant in space and time for all catchments. β was chosen as a constant to create a relatively simple approach that does not directly rely on irrigation water use data, which is beneficial for application in time periods (both historical and future), without irrigation water use data, as well as for regions where no reliable irrigation water use data is available. We estimated β by minimizing the difference between f_{IAF} and f_{IWU} in terms of Root Mean Squared Error (RMSE). We generated 1000 linearly spaced values for β between 0 and 2.5, and computed f_{IAF} for all the catchments. For all these cases, the RMSE of catchment f_{IAF} and f_{IWU} was computed (Fig. 3). The RMSE minimized for $\beta = 0.9$ ($\mathrm{RMSE} = 0.042$), which is applied for all catchments in Eq. (6).

To evaluate the effect of these methods on estimated S_{r} we tested a third case, referred to as No Irrigation (NI), in which $f_{\mathrm{NI}} = 0$. A priori we cannot and do not consider any of the two methods, i.e., the IWU or the IAF method to be more representative than the other. While the IWU method uses the irrigation data more directly than the IAF method, the latter directly takes the inter-annual variability of surplus water into account.

2.2.1 Root zone storage capacity calculation

Catchment-scale root zone storage capacity S_{r} was here derived from the catchment-scale storage deficit S_{d} timeseries for the three different irrigation cases NI, IWU, and IAF (Table 1). For each catchment, the annual maximum storage deficits ($S_{\mathrm{d,M}}$) were defined for each hydrological year as:

$$S_{\mathrm{d,M}} = \max(S_{\mathrm{d}}(t)) - \min(S_{\mathrm{d}}(t)) \quad (7)$$

with the $\min(S_{\mathrm{d}})$ occurring earlier in the hydrological year than the $\max(S_{\mathrm{d}})$. Previous studies (e.g. Gao et al., 2014; Wang-Erlandsson et al., 2016) applied a Gumbel distribution on the $S_{\mathrm{d,M}}$ values to estimate S_{r} for different return periods T. Wang-Erlandsson et al. (2016) found that for croplands, and thus irrigated land, the best evaporation simulations with a global hydrological model were achieved with an S_{r} based on a return period of 2 years, as croplands adapt to survive droughts with relatively short return periods. Here, we directly used the observed $S_{\mathrm{d,M}}$ values with occurrences closest to $T = 2$ years instead of a fitted extreme value distribution, because fitting an extreme value distribution is ambiguous for return periods of interest (here: 2 years) much smaller than the timeseries length (here: >10 years). For all catchments, for each irrigation case separately, the S_{r} was estimated as the mean of the three observed $S_{\mathrm{d,M}}$-values with occurrences closest to $T = 2$ years, as represented by the cross-markers closest to the vertical dashed line at $T = 2$ years in in Fig. 5b,d,f and h.

2.2.2 Evaluation

To visualize the effects of irrigation on S_{d} and S_{r}, we selected four example catchments with different irrigation magnitudes (i.e., I_{a} and $\overline{I_{\mathrm{w}}}$) in four different continents and climate zones. For quantification of the effects of irrigation on S_{r}, we computed absolute (Δ) and relative (Δ_{r}) differences between the S_{r} estimates for the NI, IWU and IAF cases (Table 1). Catchments were stratified based on (1) four different ranges of irrigated area I_{a}: $I_{\mathrm{a}} \leq 0.01$; $0.01 < I_{\mathrm{a}} \leq 0.05$; $0.05 < I_{\mathrm{a}} \leq 0.1$; and $I_{\mathrm{a}} > 0.1$ (Fig. S1); (2) regions, i.e., South-America, North-America, Europe and Asia; and (3) climate zones based on Köppen-Geiger, subdivided into Tropical (Af, Am, Aw), Arid (BWh, BWk, BSh, BSk), Temperate (Cfa, Cfb, Cfc), Mediterranean (Csa, Csb), and Continental (Dfa, Dfb, Dfc, Dfd) climates, with the abbrevations of the Köppen-Geiger climate classification (Beck et al., 2018a) (Fig. S2). Uncertainty of the differences in S_{r} were represented by the interquartile range (IQR).

3 Results

3.1 Irrigation influence on root zone storage capacity

Globally, the S_{r} estimates without accounting for irrigation ranged from 0–800 mm, with larger values in semi-arid regions with high rainfall seasonality such as North-Eastern Brazil (median $S_{\mathrm{r}} \approx 250\,\mathrm{mm}$) or monsoon regions such as North-Eastern Indian (median $S_{\mathrm{r}} \approx 450\,\mathrm{mm}$), than in regions with temperate climates with year-round rainfall such as Western Europe (median $S_{\mathrm{r}} \approx 70\,\mathrm{mm}$) or continental, colder, climates such as Canada (median $S_{\mathrm{r}} \approx 40\,\mathrm{mm}$) (Fig. 4).

The storage deficits S_{d} (Eq. 1) in general reduced when accounting for irrigation effects according to the IWU and IAF cases as compared to the case without irrigation (NI). These overall effects of the method are illustrated by four selected example catchments in Fig. 5. More pronounced effects of irrigation on S_{d} are visible for the example catchments in Europe (Fig. 5e,f) and Asia (Fig. 5g,h), with larger $\overline{I_{\mathrm{w}}}$ and I_{a}, than in the example catchments in South-America (Fig. 5a,b) and North-America (Fig. 5c,d). As S_{d} decreased, the annual maximum storage deficits $S_{\mathrm{d,M}}$, as determined by Eq. (7), decreased as well. Consequently, the estimated S_{r} decreased for the IWU and IAF cases compared to NI, with more pronounced effects in the example catchments with larger $\overline{I_{\mathrm{w}}}$ and I_{a} (Fig. 5). Globally, S_{r} consistently decreased for IWU and IAF (Fig. 6), albeit

the magnitudes vary to a considerable extent. Nevertheless, relatively clear regional patterns of the effects of irrigation on S_r emerged. The most pronounced effects cluster in catchments in regions that are characterized by widespread and intense crop cultivation, and thus high irrigation water use, such as Northern Spain and France and parts of India (Fig. 1).

3.2 Regional differences of irrigation influence on root zone storage capacity

Figure 7 shows that the effects of irrigation on S_r increased with increasing irrigated area fraction I_a for both IWU and IAF cases. We found the largest effects in catchments with $I_\mathrm{a} > 0.1$, such as the example catchment in Asia (Fig. 5g). For these catchments, the median ΔS_r was 19 mm (IQR 10–31 mm) for IWU and 23 mm (IQR 11–42 mm) for IAF (Fig. 7), which correspond with decreases of 12 % and 15 %, respectively (Table 2). These effects were considerably larger than the effects of irrigation in catchments with $0.05 < I_\mathrm{a} \leq 0.1$ that reached median $\Delta_\mathrm{r} S_\mathrm{r}$ of 6%, which corresponds to $\Delta S_\mathrm{r} \approx 9\,\mathrm{mm}$ (Fig. 7, Table 2). Although the median effects of irrigation on S_r for catchments with $I_\mathrm{a} \leq 0.05$ were relatively small, the effects can be considerable for specific individual catchments as shown by the outliers in Fig. 7.

The strongest irrigation influence on S_r for catchments with $I_\mathrm{a} > 0.05$ was found in Asia, followed by South-America, North-America and Europe, for both IWU and IAF (Fig. 8a). For the catchments in Asia we found median values of ΔS_r for IWU of 21 mm (IQR 13–41 mm), and for IAF of 27 mm (IQR 12–56 mm). However, the relative differences in S_r were with $\Delta_\mathrm{r} S_\mathrm{r}$ =9–10 % smaller in Asia than in other regions, reaching up to 14 % in South America, because the initial S_r without accounting for irrigation was considerably larger in Asia than in other regions (Fig. 4, Table 2). Figure 8b shows that S_r decreased the most in tropical catchments with median $\Delta S_\mathrm{r} = 19\,\mathrm{mm}$ for IWU and 24 mm for IAF. These findings are in line with the results presented in Fig. 8a since most of the tropical catchments we evaluated were located in Asia (Fig. S3). For catchments in the arid, Mediterranean, temperate, and continental climate zones, median ΔS_r was smaller and varied between 5 mm and 15 mm. However, catchments in temperate climates exhibited the largest relative influence of irrigation on S_r with median $\Delta_\mathrm{r} S_\mathrm{r}$ =14 % for IWU and 15 % for IAF (Table 2).

3.3 Comparison IWU and IAF methods

Figure 6 shows similar spatial patterns of $\Delta_\mathrm{r} S_\mathrm{r}$ for IWU and IAF, but the magnitudes differed. For most groups of catchments, IAF had a more pronounced effect on S_r than IWU (Table 2; Fig. S4). The different results for IWU and IAF can be explained by the different methodologies (Table 1). The IWU method directly used annual mean irrigation water use $\overline{I_\mathrm{w}}$ from Zhang et al. (2022) as an estimate for I, if sufficient water was available in the surplus store S_s. On the other hand, in the IAF method I was defined as a fraction of S_s based on the irrigated area fraction I_a and the constant β. Therefore, the estimated I in IAF directly reflected the inter-annual variability of surplus water. Another cause for the different results for IWU and IAF lies in the estimation of β in IAF, which was based on minimization of the differences between $f_\mathrm{i,IWU}$ and $f_\mathrm{i,IAF}$ (Sect. 2.2; Fig. 3). In spite of this optimization, differences between $f_\mathrm{i,IWU}$ and $f_\mathrm{i,IAF}$ remained, which partially explain the differences in ΔS_r between the two methods.

4 Discussion

4.1 Synthesis of results

Our results showed that the effect of irrigation on S_r is discernible in all regions, but the magnitude of the effect depends on the amount of irrigation applied (Fig. 5–8). For many parts of the world the integration of irrigation in the S_r estimation did not have a large influence (Fig. 6). However, S_r considerably reduced for catchments with irrigated area fractions $I_\mathrm{a} > 0.05$, and ignoring irrigation in these regions would lead to biased estimates of S_r, and, as a consequence, to inadequate modeling of vegetation transpiration (Fig. 7). The reduction in S_r in catchments with irrigation was expected following that the memory method is based on the theory that vegetation will invest less in roots if sufficient water is available (Guswa, 2008). The observed changes in S_r are here attributed to changes in the vegetation roots, as they are directly related to the size of S_r. Additionally, adaptations at the plant scale associated with irrigation, such as adjustments in stomatal aperture (Chaves et al., 2016) and root hydraulic conductance (Lo Gullo et al., 1998), are also implicitly related to changes in S_r. The influence of irrigation on S_r estimates, as presented in Fig. 6, resembled the spatial pattern found in global assessments of irrigation water withdrawal (Huang et al., 2018), and the extent of irrigation activities (McDermid et al., 2023). This was expected since we used similar underlying irrigation data in the here developed irrigation methods. Given the ongoing irrigation expansion as presented by McDermid et al. (2023), it is expected that larger irrigation water volumes lead to further reductions of S_r at catchment scales in the near-future compared to the reductions reported in this study. At the same time, irrigation efficiency is also improving (McDermid et al., 2023), but this effect on S_r is less straightforward. Improved irrigation efficiency (i.e., reduced soil evaporation) reduces the irrigation water volumes needed, which, at the catchment scale, leads to increased long-term mean discharge, and thus reduced long-term mean evaporation. This would result in reduced S_r in the memory method compared to a situation with lower irrigation efficiency. However, it has been shown that increased efficiency does not necessarily lead to reduced irrigation water use, as the saved water by increasing irrigation efficiency is often applied elsewhere (Grafton et al., 2018; Lankford et al., 2020).

Previous studies using the memory method did not consider irrigation in S_r estimates (e.g. De Boer-Euser et al., 2016; Stocker et al., 2023), or did not evaluate its effects (Wang-Erlandsson et al., 2016). To put our results into perspective, we looked at the effects of snow accumulation and melt on S_r estimates for the continental United States from Dralle et al. (2021), as this process alters the S_d time series in a similar way as irrigation by temporally shifting liquid water input into the system. Dralle et al. (2021) estimated that integrating snow accumulation and melt in the memory method led to an average reduction in S_r of $6\,\mathrm{mm}$ (2 %) for areas with >10 % winter snow coverage, and $28\,\mathrm{mm}$ (17 %) for areas with >80 % winter snow coverage (Dralle et al., 2020b). These magnitudes are broadly consistent with our findings for irrigation (Table 2). Our results indicate that the effects of snow and irrigation on S_r are comparable. In our study, 27 catchments have both considerable snowfall (snow days $> 5\%$ of the total days) and irrigation ($I_\mathrm{a} > 0.05$). For these catchments, the snow model (Appendix A) led on average to an S_r reduction of $7\,\mathrm{mm}$ (7%) for the NI case compared to a set-up without the snow model. With irrigation, S_r further reduced by $6\,\mathrm{mm}$ (7%), and $11\,\mathrm{mm}$ (12%) for IAF in these catchments.

Both the results of IWU and IAF showed considerable effects of irrigation on S_r (Figs. 6–8), and both are suitable to use in the memory method, keeping in mind the individual uncertainties related to data and methodological assumptions. We think that the IWU method is more suitable for regional application for periods with available I_w data (Zhang et al., 2022) than IAF, because I_w was derived from water balances, that strongly depend on the evaluated period. However, for spatial and temporal extrapolation the direct use of the I_w data in the IWU method is more uncertain than the simpler IAF method, because the irrigated area fraction I_a used in IAF is expected to be temporally less variable than the water used for irrigation I_w. Therefore, we think the simpler parameterized IAF method is more suitable to use in the memory method for global applications and varying time periods. Moreover, IAF has the potential to be integrated dynamically in hydrological or land surface models used for global Earth system model studies and future predictions.

4.2 Methodological limitations

By using several data sources, we obtained a large sample of 4856 catchments on different continents, characterized by a wide spectrum of climates, and in particular, regions with various levels of irrigation activity. However, the global coverage is not entirely balanced as Africa and large parts of Asia were undersampled. A further limitation may arise from the assumption in the memory method with irrigation methods proposed here that catchments are hydrologically closed systems. However, inter-catchment lateral flows, such as groundwater and irrigation water can significantly alter catchment water balances (e.g., Bouaziz et al., 2018; Fan, 2019; Condon et al., 2020). Moreover, the extraction of fossil groundwater for irrigation (Siebert et al., 2010; Grogan et al., 2017; de Graaf et al., 2019) can violate the assumption of closing water balances for the here developed irrigation methods in the memory method. Our methodology based on a sustainable water use assumption provides a lower boundary of S_r reduction in irrigated catchments. It is expected that irrigation exceeding sustainable use would lead to larger S_r reductions than reported here, as in this case more water is available to crops than derived from the water balance. Furthermore, the methodology assumes single succession of excess and deficit periods within a year (Fig. 2b), which is not necessarily representative in regions with double cropping systems or bimodal monsoons (Biradar and Xiao (2011)). Another limitation was the availability and quality of irrigation data (Sect. 2.1, Fig. 1). The annual mean $\overline{I_w}$ used in IWU was based on the 2011-2018 period, while the catchment time series varied between 1981 and 2010. Similarly, the I_a we used represented the 2005 irrigated area fraction (Siebert et al., 2015b). The temporal mismatch between catchment hydrological timeseries and irrigation data may have led to an overestimation of I for the catchment specific period, as irrigated area, and irrigation techniques and efficiency have developed over the evaluated period (McDermid et al., 2023). Although this inconsistency in the temporal data influences the catchment specific outcomes, we believe that it did not have major influence the quantification of the general patterns of the effects of irrigation on S_r, which was the aim of this study.

An additional source of uncertainty in the application of the memory method, as used in this study, relates to the derivation of S_r from the S_d time series (Fig. 5). Given that an ecosystem has developed its S_r in a way it optimally functions and can overcome dry periods (e.g. Guswa, 2008), S_r for a specific time period would correspond to the maximum S_d value observed during that same time period ($S_r = \max(S_d)$). However, it is important to note that the memory method represents a simplified approximation of real ecosystem behavior and has inherent limitations. The most important limitation is that our application of

the memory method did not account for the feedback between S_d and $E_\mathrm{t}/E_\mathrm{p}$, which likely led to an overestimation of S_d (Van Oorschot et al., 2021). In this study, we primarily focused on crops, that do not exhibit a multi-year root adaptation for survival, as there is no remaining S_r after each year's harvest. However, the catchments used here are in no case entirely covered by crops, and, therefore, we used a return period of 2 years for the S_r estimation (following Wang-Erlandsson et al. (2016)).

5 Conclusions

Using a large sample of catchments globally, the presented results support the hypothesis that irrigation considerably reduces root zone storage capacity S_r estimated with the memory method. We found a median reduction of S_r by 12 % (IQR 7–21 %) for the IWU method and 15 % (IQR 6–33 %) for the IAF method for catchments with an irrigated area fraction I_a >10 %. In general, these effects were less pronounced in catchments with a smaller irrigated area, although the S_r for individual catchments could also be considerably influenced by irrigation. S_r decreased the most for catchments in tropical climates with a median decrease of 19–24 mm (for I_a >5 %). The reductions of S_r found in this study are in the same order of magnitude as the snow effects on S_r estimated by Dralle et al. (2021). Of paramount relevance for regional-to-global hydrological and climate modelling studies, this study demonstrates the relevance of irrigation for adequately estimating S_r. The irrigation water use can be expected to further increase over the next decades and so the related effects on S_r should be represented in the Earth system models that are used for the next climate projections. The methodological approach developed in this study could be profitably used in this respect.

Code and data availability. GSIM discharge data was obtained from https://doi.pangaea.de/10.1594/PANGAEA.887477 (Do et al., 2018) and https://doi.pangaea.de/10.1594/PANGAEA.887470 (Gudmundsson et al., 2018), CAMELS-AUS data from https://doi.pangaea.de/10.1594/PANGAEA.921850 (Fowler et al., 2020), LamaH-CE data from https://zenodo.org/record/7691294 (Kauzlaric et al., 2023), discharge data for Italian catchments from http://meteoniardo.altervista.org/ (Lendvai, 2020). GSWP3 precipitation and daily mean temperature were obtained from https://data.isimip.org/search/simulation_round/ISIMIP2a/product/InputData/climate_forcing/gswp3/ (Lange and Büchner, 2020) and potential evaporation from GLEAM v3.5a was downloaded from https://www.gleam.eu/#downloads (Miralles et al., 2011; Martens et al., 2017). Irrigated area fraction was downloaded from https://mygeohub.org/publications/8/2 (Siebert et al., 2015a) and irrigation water use from https://data.tpdc.ac.cn/en/data/ad558954-bc55-44cf-94c8-bdb33820f784/ (Xin et al., 2021). The global map of the Köppen-Geiger climate classification was obtained from https://figshare.com/articles/dataset/Present_and_future_K_ppen-Geiger_climate_classification_maps_at_1-km_resolution/6396959/2 (Beck et al., 2018b). Upon acceptance, the data and scripts underlying this manuscript will be shared in an open access research database.

Appendix A: Memory method equations

These equations follow Van Oorschot et al. (2021), who based their methods on Gao et al. (2014); De Boer-Euser et al. (2016); Nijzink et al. (2016) and Wang-Erlandsson et al. (2016). Total precipitation (P ($\mathrm{mm\,day^{-1}}$)) was split into liquid precipitation

(P_l ($\mathrm{mm\,day^{-1}}$)), and precipitation falling as snow (P_sn ($\mathrm{mm\,day^{-1}}$)) based on temperature (Fig. 2). As temperature varies with altitude, we divided each catchment in elevation zones of 250 m. For each elevation zone z the daily temperature T_z was calculated by:

$$T_z(t) = T_\mathrm{a}(t) + \lambda \Delta H \tag{A1}$$

with T_a (°C) the catchment average temperature (GSWP3), λ the lapse rate of $0.0064\,^\circ\mathrm{C\,m^{-1}}$, and ΔH (m) the elevation difference between the elevation zone and the mean elevation. For each elevation zone z daily P_l and P_sn were defined by:

$$P_{\mathrm{l},z}(t) = \begin{cases} P(t) & \text{if } T_z(t) > T_\mathrm{t} \\ 0 & \text{if } T_z(t) < T_\mathrm{t} \end{cases} \tag{A2}$$

$$P_{\mathrm{sn},z}(t) = \begin{cases} P(t) & \text{if } T_z(t) < T_\mathrm{t} \\ 0 & \text{if } T_z(t) > T_\mathrm{t} \end{cases} \tag{A3}$$

The water balance of the snow storage (S_sn) (Fig. 2) for each elevation zone z was described by:

$$\frac{\mathrm{d}S_{\mathrm{sn},z}}{\mathrm{d}t} = P_{\mathrm{sn},z} - P_{\mathrm{m},z}. \tag{A4}$$

Equation (A4) can be solved by Eqs. (A5) and (A6), in which we used for the sum of fluxes between two time steps the following notation: $F_t = \int_{t-1}^{t} F \mathrm{d}t$, where F is either P_sn or P_m. Thus, the numerical solution using daily time steps can be described as:

$$S_{\mathrm{sn},z,t} = S_{\mathrm{sn},z,t-1} + P_{\mathrm{sn},z,t} - P_{\mathrm{m},z,t} \tag{A5}$$

$$P_{\mathrm{m},z,t} = \begin{cases} \max(M(T_{z,t} - T_\mathrm{t}),\, S_{\mathrm{sn},z,t}) & \text{if } T_{z,t} < T_\mathrm{t} \\ 0 & \text{if } T_{z,t} > T_\mathrm{t} \end{cases} \tag{A6}$$

with T_t the threshold temperature for snowfall of 0 °C, and M the snow melt factor of $2\,\mathrm{mm\,d^{-1}\,^\circ C^{-1}}$. Total catchment P_l, P_sn, and P_m were calculated as an area weighted sum of the values for the different elevation zones.

The calculation of effective precipitation P_e ($\mathrm{mm\,day^{-1}}$) and transpiration E_t in Eq. (1) are similar as in Van Oorschot et al. (2021). The water balance of the interception store S_i (Fig. 2a) is described by:

$$\frac{\mathrm{d}S_\mathrm{i}}{\mathrm{d}t} = P_\mathrm{l} - P_\mathrm{e} - E_\mathrm{i} \tag{A7}$$

with P_l the liquid precipitation ($\mathrm{mm\,day^{-1}}$) and E_i the interception evaporation ($\mathrm{mm\,day^{-1}}$). Equation (A7) can be solved by Eqs. (A8)-(A10), in which we used for the sum of fluxes between two time steps the following notation: $F_t = \int_{t-1}^{t} F \mathrm{d}t$, where

F is either P_l, E_i, P_e or E_p (potential evaporation ($\mathrm{mm\,day^{-1}}$)). Thus, the numerical solution using daily time steps can be described as:

$$P_{\mathrm{e},t} = \begin{cases} 0 & \text{if } P_{\mathrm{l},t} + S_{\mathrm{i},t-1} \leq S_{\mathrm{i,max}} \\ P_{\mathrm{l},t} + S_{\mathrm{i},t-1} - S_{\mathrm{i,max}} & \text{if } P_{\mathrm{l},t} + S_{\mathrm{i},t-1} > S_{\mathrm{i,max}} \end{cases} \tag{A8}$$

$$S^*_{\mathrm{i},t} = S_{\mathrm{i},t-1} + P_{\mathrm{l},t} - P_{\mathrm{e},t} \tag{A9}$$

$$E_{\mathrm{i},t} = \begin{cases} E_{\mathrm{p},t} & \text{if } E_{\mathrm{p},t} < S^*_{\mathrm{i},t} \\ S^*_{\mathrm{i},t} & \text{if } E_{\mathrm{p},t} \geq S^*_{\mathrm{i},t} \end{cases} \tag{A10}$$

with E_p potential evaporation ($\mathrm{mm\,day^{-1}}$) and $S_\mathrm{i,max}$ the maximum interception storage (mm). The size of $S_\mathrm{i,max}$ has minor influence on estimates of S_r as shown by e.g. Hrachowitz et al. (2021) and Bouaziz et al. (2020), and was, therefore, set to a constant value of 2.5 mm. Daily transpiration (E_t) in Eq. (1) was calculated as a fraction of daily E_p by:

$$E_\mathrm{t} = (E_\mathrm{p} - E_\mathrm{i}) \frac{\overline{E_\mathrm{t}}}{\overline{E_\mathrm{p}} - \overline{E_\mathrm{i}}} \tag{A11}$$

with $\overline{E_\mathrm{t}}$ the long-term mean E_t derived from the water balance ($\overline{E_\mathrm{t}} = \overline{P_\mathrm{e}} - \overline{Q}$), and $\overline{E_\mathrm{p}}$ the long-term mean E_p.

Author contributions. FO conceptualized the study and carried out the formal analysis with input from RE and MH. FO prepared the manuscript with contributions from RE, MH and AA.

Competing interests. MH is member of the Editorial Board of HESS. The authors have no other competing interests to declare.

Disclaimer. TEXT

Acknowledgements. This work was supported by Netherlands Organization for Scientific Research (NWO) under grant OCENW.XS22.2.109, and by the European Union's Horizon 2020 research and innovation program under grant agreement no. 101004156 (CONFESS project). Acknowledgement is given for the use of the DelftBlue computing facility at the Delft High Performance Computing Center (DHPC) (Delft High Performance Computing Centre , DHPC).

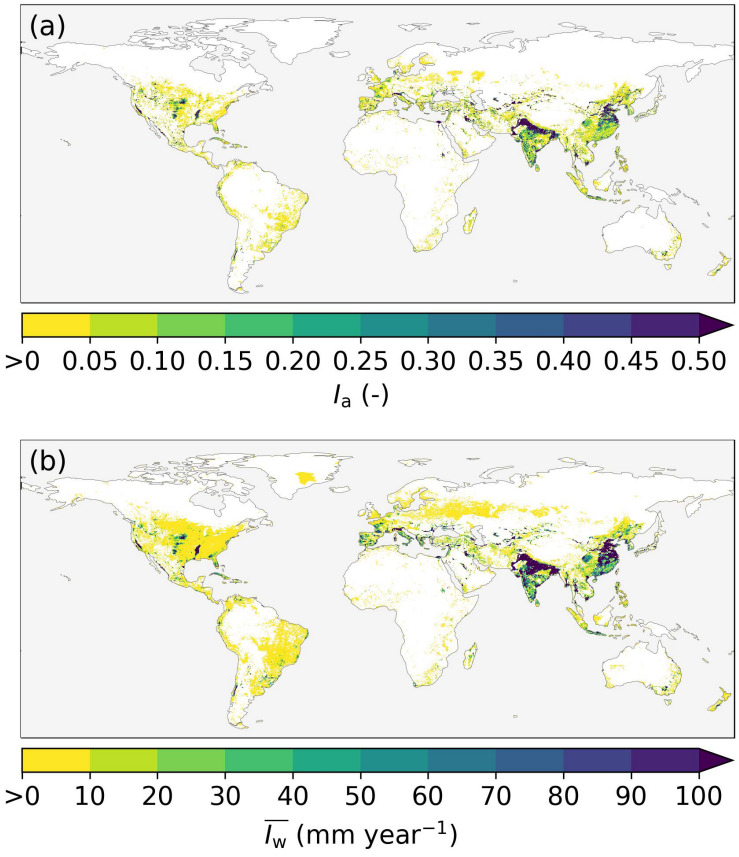

Figure 1. Global irrigation characteristics. (a) Irrigated area fraction (I_a (-)) representative for 2005 based on sub-national irrigation statistics and the HYDE 3.1 land use data (Siebert et al., 2015b). (b) Annual mean irrigation water use ($\overline{I_w}$ ($\mathrm{mm\,year^{-1}}$)) for the period 2011-2018 based on multiple satellite-based products and the PT-JPL model (Zhang et al., 2022). White areas indicate I_a or $\overline{I_w}$ equal to zero.

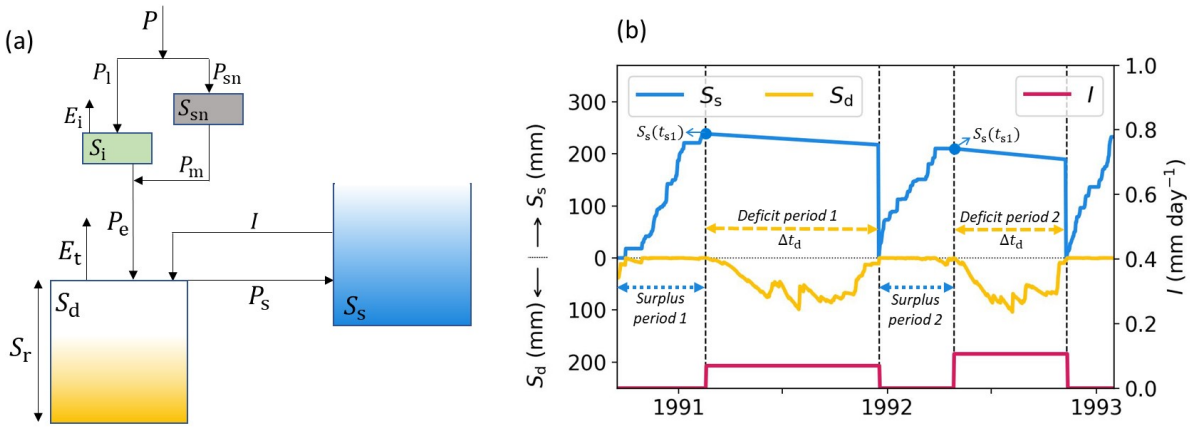

Figure 2. (a) Schematic bucket model representation of the memory method including an irrigation model with the following storages (mm): interception storage (S_i), snow storage (S_sn), storage deficit (S_d), surplus storage (S_s), and root zone storage capacity (S_r); and fluxes (mm day^{-1}): total precipitation (P), liquid precipitation (P_l), precipitation falling as snow (P_sn), interception evaporation (E_i), snow melt (P_m), effective precipitation (P_e), transpiration (E_t), precipitation surplus (P_s) and irrigation (I). (b) An example time series of S_s, S_d and I based on Eqs. (1–6), with Δt_d the length of the deficit period (days), and $S_\mathrm{s}(t_{\mathrm{s}1})$ the surplus storage at the end of the surplus period. Note that this time series represents only two years to illustrate the method, while all catchments have at least ten years of data.

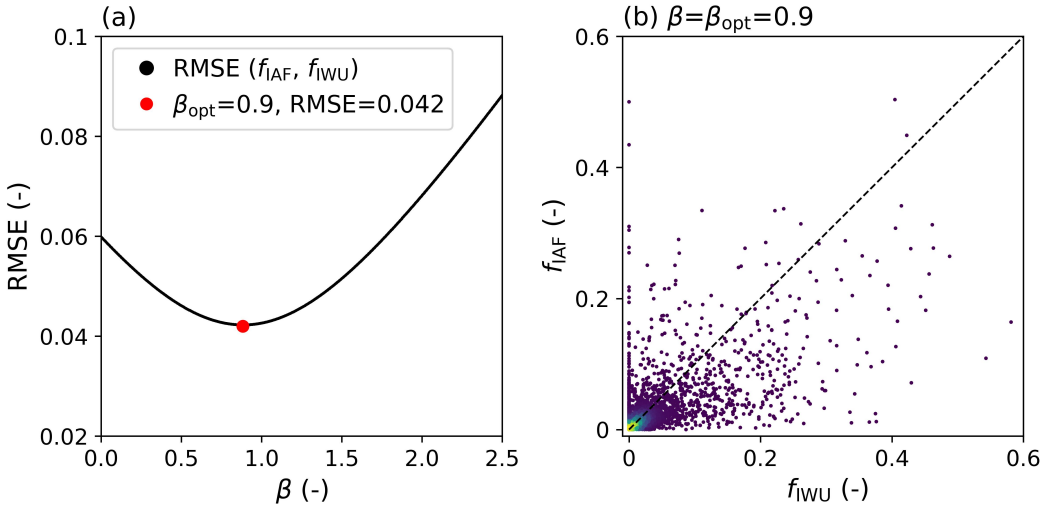

Figure 3. Root Mean Squared Error (RMSE) between the catchment irrigation factors f_{IWU} (Eq. 5) and f_{IAF} (Eq. 6) for 4856 catchments for 1000 linearly spaced values of β between 0 and 2.5. β_{opt} represents the value for β where the RMSE minimizes. (b) Scatter of f_{IWU} (Eq. 5) and f_{IAF} (Eq. 6) for β=β_{opt}=0.9 with lighter colours indicating a higher point density.

Table 1. Details of the irrigation cases considered in this study.

Irrigation case	Details	Irrigation factor f (Eq. (4))
NI	No irrigation	$f_{\mathrm{NI}} = 0$
IWU	Irrigation based on Irrigation Water Use (Fig. 1b)	$f_{\mathrm{IWU}} = \max(1, \frac{\overline{I_{\mathrm{w}}}\mathrm{d}t}{S_{\mathrm{s}}(t_{s,1})})$ (Eq. (5))
IAF	Irrigation based on Irrigated Area Fraction I_{a} (Fig. 1a)	$f_{\mathrm{IAF}} = \beta I_{\mathrm{a}}$ (Eq. (6))

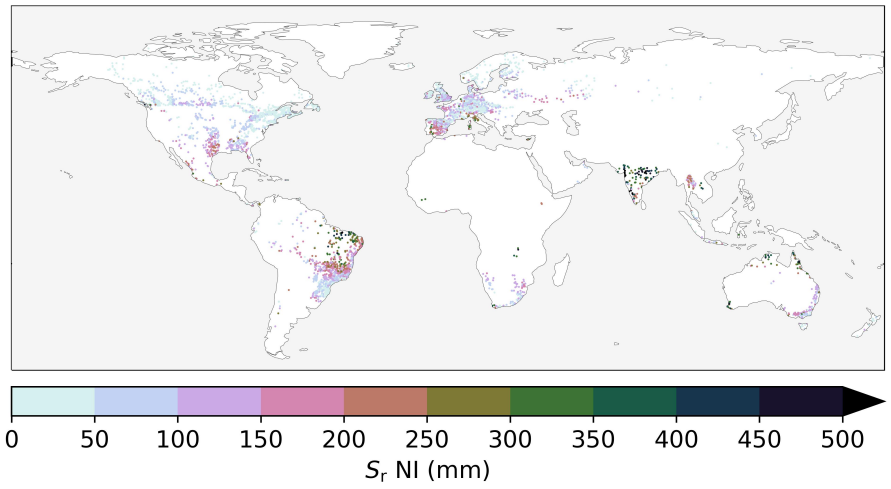

Figure 4. Catchment S_r for the No Irrigation (NI) case, with dots representing catchment outlets. Similar figures for the IWU and IAF cases are presented in Fig. S3.

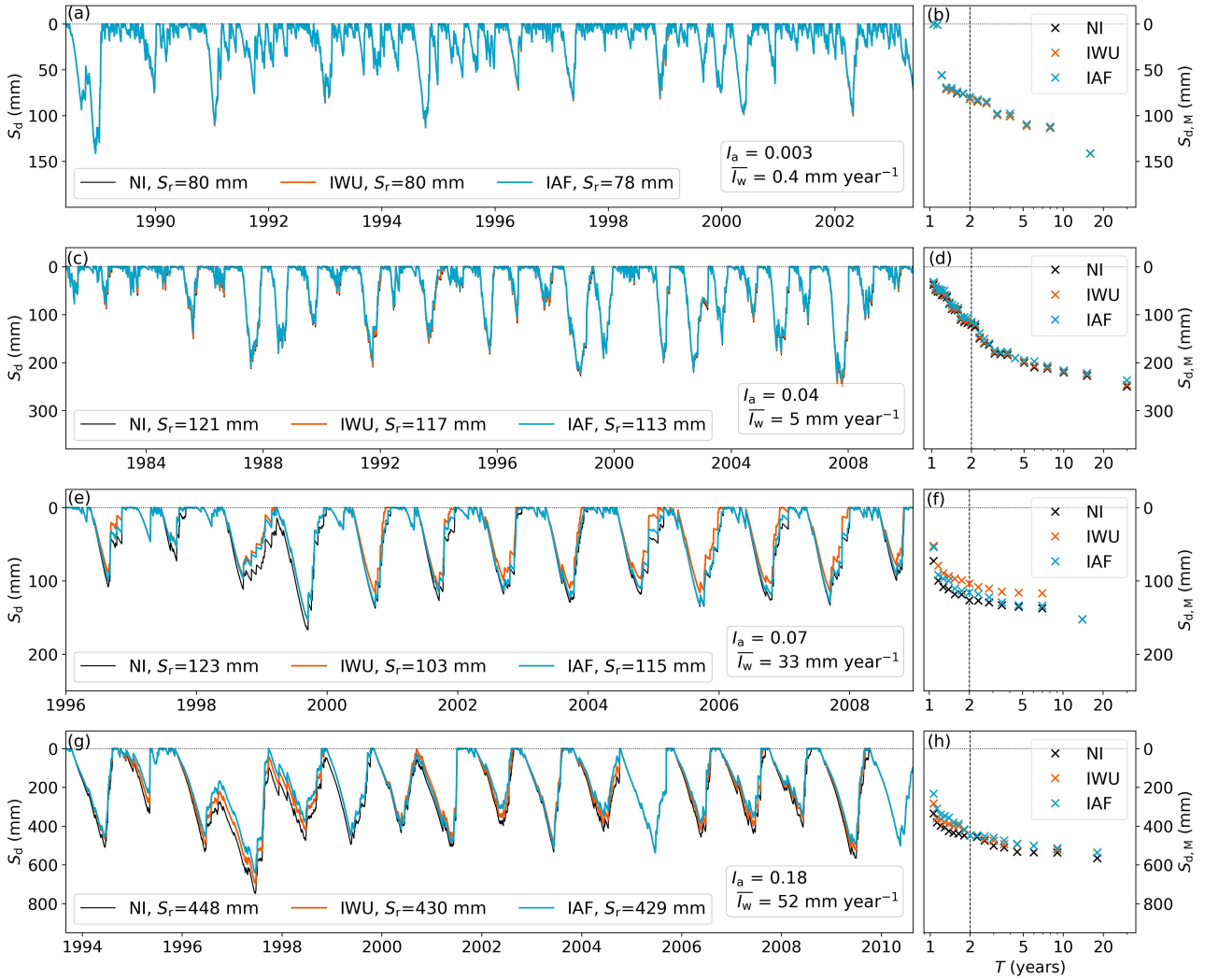

Figure 5. (a, c, e, g) Timeseries of storage deficits S_d (mm) (Eq. 1) for four illustrative catchments with increasing irrigation from top to bottom for the three irrigation cases NI, IWU, and IAF (Table 1) with for each catchment the associated annual mean irrigation water use ($\overline{I_\mathrm{w}}$), irrigated area fraction (I_a), and root zone storage capacity (S_r) values. (b, d, f, h) Return level plot of annual maximum storage deficits ($S_{\mathrm{d,M}}$) (Eq. 7) for the three irrigation cases NI, IWU and IAF with the dashed vertical line corresponding to a return period T of 2 years (Section 2.2.1). The locations of the catchments are shown in Fig. 6. Catchment identity, continent, and Köppen Geiger climate zone are from top to bottom: br_0002356, South America, temperate (Cfb); ca_0000689, North America, continental (Dfb); es_0000742, Europe, Mediterranean (Csa); in_0000252, Asia, tropical (Aw).

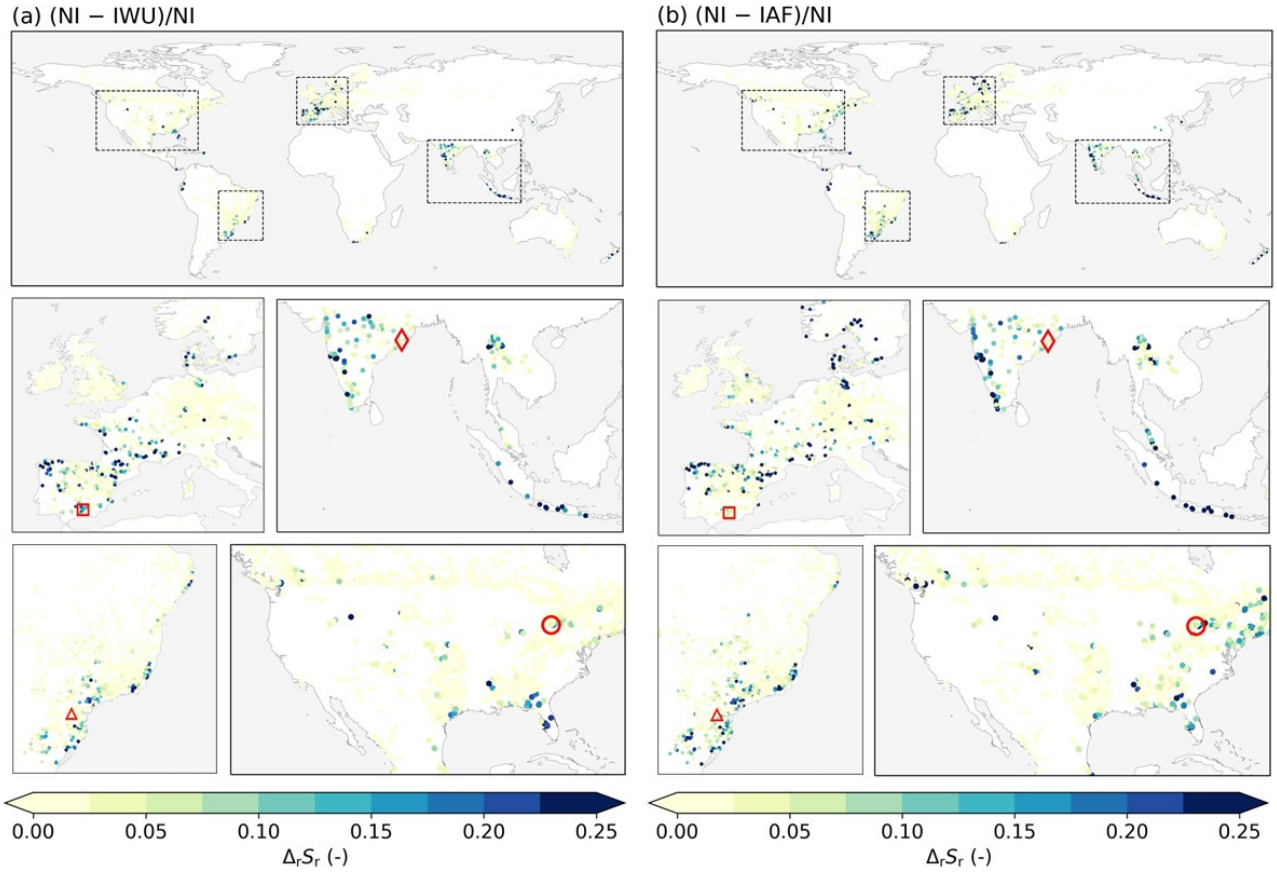

Figure 6. Relative difference in S_r ($\Delta_\mathrm{r}S_\mathrm{r}$ (-)) for (a) IWU compared to NI ((NI-IWU)/NI) and (b) IAF compared to NI ((NI-IAF)/NI). Red markers indicate the selected catchments from Fig. 5. See Table 1 for details on the irrigation cases.

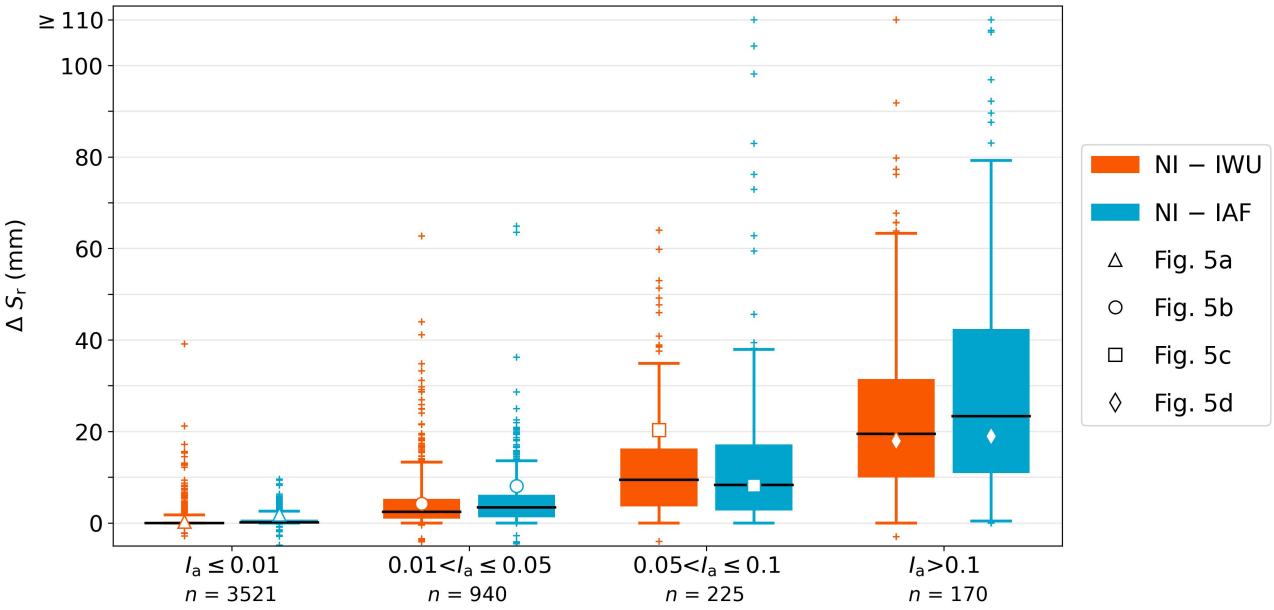

Figure 7. Boxplots of absolute S_r difference ($\Delta Sr\,(\mathrm{mm})$) between the irrigation cases (IWU and IAF) and the no irrigation case (NI) (Table 1). Catchments are stratified in four groups based on the irrigated area fraction I_a (Fig. S2), with n the number of catchments in each group. The black line represents the median, the box the interquartile range (IQR), and the whiskers the 5th and 95th percentiles. White markers represent the points presented in Fig. 5. Median and IQR values for relative S_r differences ($\Delta_r Sr\,(\%)$) are presented in Table 2.

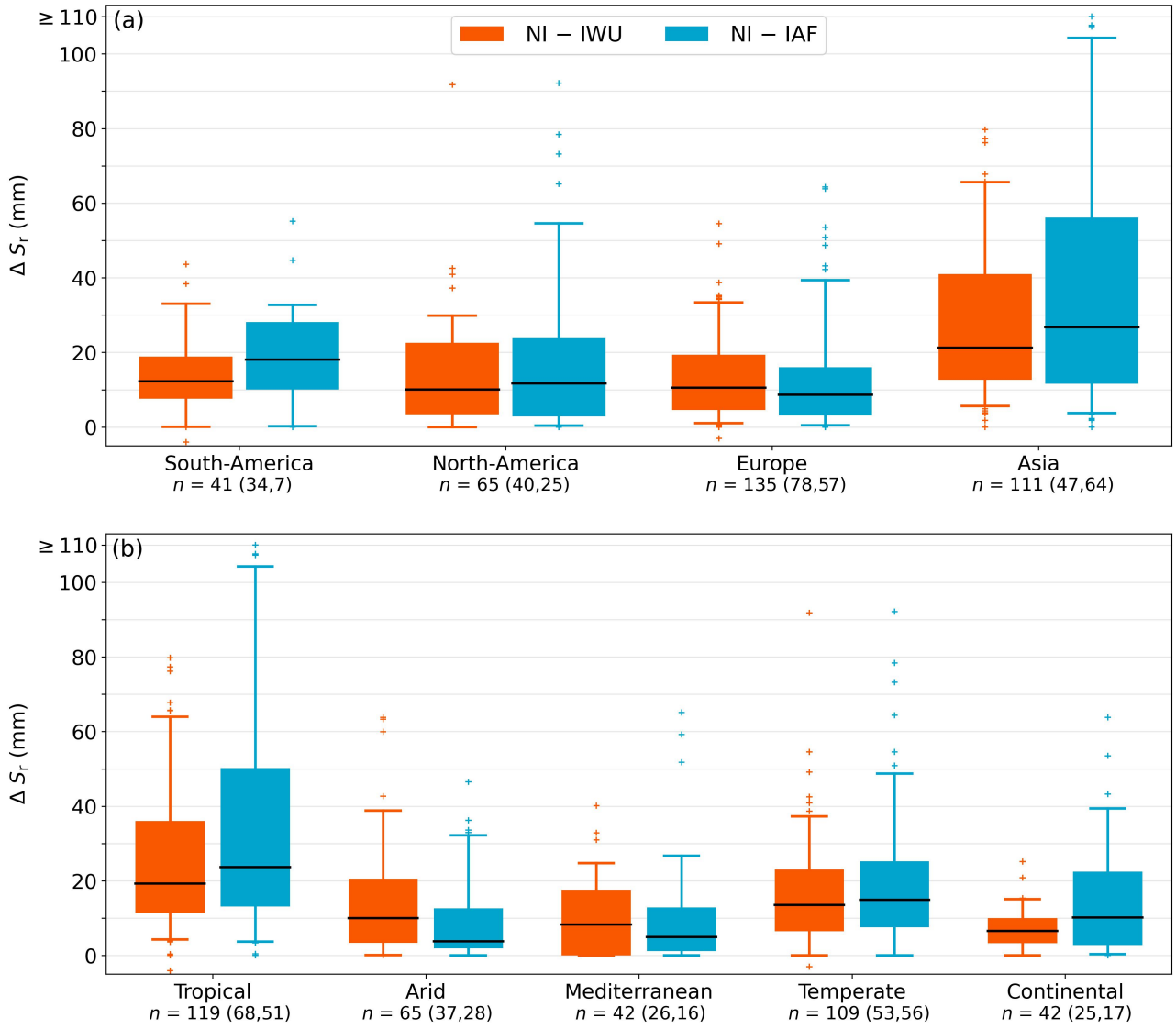

Figure 8. Boxplots of absolute S_r difference ($\Delta S_r\,(\mathrm{mm})$) between the irrigation cases (IWU and IAF) and the no irrigation case (NI) (Table 1). In (a) catchments are stratified regionally, similar to the maps in Fig. 6, and in (b) catchments are stratified based on climate zone (Sect. 2.2.2, Fig. S3), with for both (a) and (b) only catchments with irrigated area fraction $I_a > 0.05$. The total number of catchments (n) in each group is given, with the numbers in brackets representing n in $0.05 < I_a \leq 0.1$, and $I_a > 0.1$, respectively. The black line represents the median, the box the interquartile range (IQR), and the whiskers the 5th and 95th percentiles. Median and IQR values for relative S_r differences ($\Delta_r Sr\,(\%)$) are presented in Table 2.

Table 2. Median and interquartile range (IQR) of the relative S_r difference ($\Delta_\mathrm{r} S\mathrm{r}\,(\%)$) between the irrigation cases (IWU and IAF) and the no irrigation case (NI) with the catchments stratified for the top four rows based on irrigated area fraction (I_a) (Fig. 7), for the middle four rows based on region (only catchments with $I_\mathrm{a} > 0.05$) (Fig. 8a), and for the bottom five rows based on climate zones (only catchments with $I_\mathrm{a} > 0.05$) (Fig. 8b). IQR is given as the 25th percentile – 75th percentile.

	(NI–IWU)/NI		(NI–IAF)/NI	
	median	IQR	median	IQR
$I_\mathrm{a} \leq 0.01$	0	0–0	0	0–1
$0.01 < I_\mathrm{a} \leq 0.05$	2	1–6	3	1–8
$0.05 < I_\mathrm{a} \leq 0.1$	6	3–14	6	2–17
$I_\mathrm{a} > 0.1$	12	7–21	15	6–33
South-America	12	7–20	14	8–29
North-America	9	3–16	11	3–23
Europe	9	4–19	7	2–26
Asia	9	5–16	10	4–21
Tropical	9	5–17	10	5–26
Arid	5	2–11	3	1–7
Mediterranean	5	0–10	3	1–8
Temperate	14	6–23	15	6–33
Continental	8	4–12	22	4–34

References

Alexandratos, N. and Bruinsma, J.: World agriculture towards 2030/2050: the 2012 revision, Food and Agricultural Organization of the United Nation, https://doi.org/10.22004/ag.econ.288998, 2012.

Bakker, M. R., Jolicoeur, E., Trichet, P., Augusto, L., Plassard, C., Guinberteau, J., and Loustau, D.: Adaptation of fine roots to annual fertilization and irrigation in a 13-year-old Pinus pinaster stand, Tree Physiology, 29, 229–238, https://doi.org/10.1093/treephys/tpn020, 2009.

Beck, H. E., Zimmermann, N. E., McVicar, T. R., Vergopolan, N., Berg, A., and Wood, E. F.: Present and future Köppen-Geiger climate classification maps at 1-km resolution, https://doi.org/10.6084/m9.figshare.6396959, 2018a.

Beck, H. E., Zimmermann, N. E., McVicar, T. R., Vergopolan, N., Berg, A., and Wood, E. F.: Present and future köppen-geiger climate classification maps at 1-km resolution, Scientific Data, 5, 1–12, https://doi.org/10.1038/sdata.2018.214, 2018b.

Bergstrom, S.: The development of a snow routine for the HBV-2 model, Nordic Hydrology, pp. 73–92, https://doi.org/10.2166/nh.1975.0006, 1975.

Biradar, C. M. and Xiao, X.: Quantifying the area and spatial distribution of double- and triple-cropping croplands in India with multi-temporal MODIS imagery in 2005, International Journal of Remote Sensing, 32, 367–386, https://doi.org/10.1080/01431160903464179, 2011.

Bouaziz, L., Weerts, A., Schellekens, J., Sprokkereef, E., Stam, J., Savenije, H., and Hrachowitz, M.: Redressing the balance: Quantifying net intercatchment groundwater flows, Hydrology and Earth System Sciences, 22, 6415–6434, https://doi.org/10.5194/hess-22-6415-2018, 2018.

Bouaziz, L. J., Steele-Dunne, S. C., Schellekens, J., Weerts, A. H., Stam, J., Sprokkereef, E., Winsemius, H. H., Savenije, H. H., and Hrachowitz, M.: Improved Understanding of the Link Between Catchment-Scale Vegetation Accessible Storage and Satellite-Derived Soil Water Index, Water Resources Research, 56, 1–22, https://doi.org/10.1029/2019WR026365, 2020.

Bouaziz, L. J. E., Aalbers, E. E., Weerts, A. H., Hegnauer, M., Buiteveld, H., Lammersen, R., Stam, J., Sprokkereef, E., Savenije, H. H. G., and Hrachowitz, M.: Ecosystem adaptation to climate change: the sensitivity of hydrological predictions to time-dynamic model parameters, Hydrology and Earth System Sciences, 26, 1295–1318, https://doi.org/10.5194/hess-26-1295-2022, 2022.

Brunner, I., Herzog, C., Dawes, M. A., Arend, M., and Sperisen, C.: How tree roots respond to drought, Frontiers in Plant Science, 6, https://doi.org/10.3389/fpls.2015.00547, 2015.

Chaves, M., Costa, J., Zarrouk, O., Pinheiro, C., Lopes, C., and Pereira, J.: Controlling stomatal aperture in semi-arid regions—The dilemma of saving water or being cool?, Plant Science, 251, 54–64, https://doi.org/10.1016/j.plantsci.2016.06.015, special Issue: Water-Use Efficiency in Plants, 2016.

Collins, D. B. and Bras, R. L.: Plant rooting strategies in water-limited ecosystems, Water Resources Research, 43, 1–10, https://doi.org/10.1029/2006WR005541, 2007.

Condon, L. E., Markovich, K. H., Kelleher, C. A., McDonnell, J. J., Ferguson, G., and McIntosh, J. C.: Where Is the Bottom of a Watershed?, Water Resources Research, 56, e2019WR026 010, https://doi.org/https://doi.org/10.1029/2019WR026010, e2019WR026010 2019WR026010, 2020.

De Boer-Euser, T., McMillan, H. K., Hrachowitz, M., Winsemius, H. C., and Savenije, H. H.: Influence of soil and climate on root zone storage capacity, Water Resources Research, 52, 2009–2024, https://doi.org/10.1002/2015WR018115, 2016.

de Boer-Euser, T., Meriö, L.-J., and Marttila, H.: Controls on root zone storage capacity in boreal regions, Hydrology and Earth System Sciences Discussions, pp. 1–20, https://doi.org/10.5194/hess-2018-87, 2018.

de Graaf, I. E., Gleeson, T., Van Beek, L., Sutanudjaja, E. H., and Bierkens, M. F.: Environmental flow limits to global groundwater pumping, Nature, 574, 90–94, https://doi.org/10.1038/s41586-019-1594-4, 2019.

Delft High Performance Computing Centre (DHPC): DelftBlue Supercomputer (Phase 1), https://www.tudelft.nl/dhpc/ark:/44463/DelftBluePhase1, 2022.

Dirmeyer, P., Gao, X., Zhao, M., Guo, Z., Oki, T., and Hanasaki, N.: GSWP-2: Multimodel Analysis and Implications for Our Perception of the Land Surface, Bulletin of The American Meteorological Society, 87, https://doi.org/10.1175/BAMS-87-10-1381, 2006.

Do, H. X., Gudmundsson, L., Leonard, M., and Westra, S.: The Global Streamflow Indices and Metadata Archive (GSIM)-Part 1: The production of a daily streamflow archive and metadata, Earth System Science Data, 10, 765–785, https://doi.org/10.5194/essd-10-765-2018, 2018.

Do, H. X., Gudmundsson, L., Leonard, M., and Westra, S.: The Global Streamflow Indices and Metadata Archive - Part 1: Station catalog and Catchment boundary, https://doi.org/10.1594/PANGAEA.887477, 2018.

Dralle, D. N., Hahm, W., Rempe, D. M., Karst, N., Anderegg, L. D., Thompson, S. E., Dawson, T. E., and Dietrich, W. E.: Plants as sensors: Vegetation response to rainfall predicts root-zone water storage capacity in Mediterranean-type climates, Environmental Research Letters, 15, https://doi.org/10.1088/1748-9326/abb10b, 2020a.

Dralle, D. N., Hahm, W. J., and Rempe, D. M.: Dataset for "Accounting for snow in the estimation of root-zone water storage capacity from precipitation and evapotranspiration fluxes", HydroShare, http://www.hydroshare.org/resource/ee45c2f5f13042ca85bcb86bbfc9dd37, 2020b.

Dralle, D. N., Hahm, W. J., Chadwick, K. D., McCormick, E., and Rempe, D. M.: Technical note: Accounting for snow in the estimation of root zone water storage capacity from precipitation and evapotranspiration fluxes, Hydrology and Earth System Sciences, 25, 2861–2867, https://doi.org/10.5194/hess-25-2861-2021, 2021.

Engels, C., Mollenkopf, M., and Marschner, H.: Effect of drying and rewetting the topsoil on root growth of maize and rape in different soil depths, Zeitschrift für Pflanzenernährung und Bodenkunde, 157, 139–144, https://doi.org/10.1002/jpln.19941570213, 1994.

Fan, Y.: Are catchments leaky?, WIREs Water, 6, e1386, https://doi.org/https://doi.org/10.1002/wat2.1386, 2019.

Fan, Y., Miguez-Macho, G., Jobbágy, E. G., Jackson, R. B., and Otero-Casal, C.: Hydrologic regulation of plant rooting depth, Proceedings of the National Academy of Sciences, 114, 10 572–10 577, https://doi.org/10.1073/pnas.1712381114, 2017.

FAO: World Food and Agriculture - Statistical Yearbook 2022, FAO, https://doi.org/10.4060/cc2211en, 2022.

Fowler, K., Acharya, S. C., Addor, N., Chou, C., and Peel, M.: CAMELS-AUS v1: Hydrometeorological time series and landscape attributes for 222 catchments in Australia, https://doi.org/10.1594/PANGAEA.921850, 2020.

Fowler, K. J., Acharya, S. C., Addor, N., Chou, C., and Peel, M. C.: CAMELS-AUS: Hydrometeorological time series and landscape attributes for 222 catchments in Australia, Earth System Science Data, 13, 3847–3867, https://doi.org/10.5194/essd-13-3847-2021, 2021.

Gao, H., Hrachowitz, M., Schymanski, S. J., Fenicia, F., Sriwongsitanon, N., and Savenije, H.: Climate controls how ecosystems size the root zone storage capacity at catchment scale, Geophysical Research Letters, 41, 7916–7923, https://doi.org/10.1002/2014GL061668, 2014.

Gao, H., Ding, Y., Zhao, Q., Hrachowitz, M., and Savenije, H. H.: The importance of aspect for modelling the hydrological response in a glacier catchment in Central Asia, Hydrological Processes, 31, 2842–2859, https://doi.org/https://doi.org/10.1002/hyp.11224, 2017.

Gentine, P., D'Odorico, P., Lintner, B. R., Sivandran, G., and Salvucci, G.: Interdependence of climate, soil, and vegetation as constrained by the Budyko curve, Geophysical Research Letters, 39, 2–7, https://doi.org/10.1029/2012GL053492, 2012.

Grafton, R. Q., Williams, J., Perry, C. J., Molle, F., Ringler, C., Steduto, P., Udall, B., Wheeler, S. A., Wang, Y., Garrick, D., and Allen, R. G.: The paradox of irrigation efficiency, Science, 361, 748–750, https://doi.org/10.1126/science.aat9314, 2018.

Grogan, D. S., Wisser, D., Prusevich, A., Lammers, R. B., and Frolking, S.: The use and re-use of unsustainable groundwater for irrigation: a global budget, Environmental Research Letters, 12, 034 017, https://doi.org/10.1088/1748-9326/aa5fb2, 2017.

Gudmundsson, L., Do, H. X., Leonard, M., and Westra, S.: The Global Streamflow Indices and Metadata Archive (GSIM)-Part 2: Quality control, time-series indices and homogeneity assessment, Earth System Science Data, 10, 787–804, https://doi.org/10.5194/essd-10-787-2018, 2018.

Gudmundsson, L., Do, H. X., Leonard, M., and Westra, S.: The Global Streamflow Indices and Metadata Archive (GSIM) - Part 2: Time Series Indices and Homogeneity Assessment, https://doi.org/10.1594/PANGAEA.887470, 2018.

Guswa, A. J.: The influence of climate on root depth: A carbon cost-benefit analysis, Water Resources Research, 44, 1–11, https://doi.org/10.1029/2007WR006384, 2008.

Hrachowitz, M., Stockinger, M., Coenders-Gerrits, M., Van Der Ent, R., Bogena, H., Lücke, A., and Stumpp, C.: Reduction of vegetation-accessible water storage capacity after deforestation affects catchment travel time distributions and increases young water fractions in a headwater catchment, Hydrology and Earth System Sciences, 25, 4887–4915, https://doi.org/10.5194/hess-25-4887-2021, 2021.

Huang, Z., Hejazi, M., Li, X., Tang, Q., Vernon, C., Leng, G., Liu, Y., Döll, P., Eisner, S., Gerten, D., Hanasaki, N., and Wada, Y.: Reconstruction of global gridded monthly sectoral water withdrawals for 1971-2010 and analysis of their spatiotemporal patterns, Hydrology and Earth System Sciences, 22, 2117–2133, https://doi.org/10.5194/hess-22-2117-2018, 2018.

Jägermeyr, J., Gerten, D., Heinke, J., Schaphoff, S., Kummu, M., and Lucht, W.: Water savings potentials of irrigation systems: global simulation of processes and linkages, Hydrology and Earth System Sciences, 19, 3073–3091, https://doi.org/10.5194/hess-19-3073-2015, 2015.

Jha, S. K., Gao, Y., Liu, H., Huang, Z., Wang, G., Liang, Y., and Duan, A.: Root development and water uptake in winter wheat under different irrigation methods and scheduling for North China, Agricultural Water Management, 182, 139–150, https://doi.org/10.1016/j.agwat.2016.12.015, 2017.

Kauzlaric, M., Schürmann, S., Ummel, D., and Zischg, A.: Hourly discharge database HydroCH, https://doi.org/10.5281/zenodo.7691294, 2023.

Kleidon, A.: Global datasets of rooting zone depth inferred from inverse methods, Journal of Climate, 17, 2714–2722, https://doi.org/10.1175/1520-0442(2004)017<2714:GDORZD>2.0.CO;2, 2004.

Kleidon, A. and Heimann, M.: A method of determining rooting depth from a terrestrial biosphere model and its impacts on the global water and carbon cycle, Global Change Biology, 4, 275–286, https://doi.org/10.1046/j.1365-2486.1998.00152.x, 1998.

Klein Goldewijk, K., Beusen, A., van Drecht, G., and de Vos, M.: The HYDE 3.1 spatially explicit database of human-induced global land-use change over the past 12,000 years, Global Ecology and Biogeography, 20, 73–86, https://doi.org/https://doi.org/10.1111/j.1466-8238.2010.00587.x, 2011.

Klepper, B.: Crop root system response to irrigation, Irrigation Science, 12, 105–108, https://doi.org/10.1007/BF00192280, 1991.

Klingler, C., Schulz, K., and Herrnegger, M.: LamaH-CE: LArge-SaMple DAta for Hydrology and Environmental Sciences for Central Europe, Earth System Science Data, 13, 4529–4565, https://doi.org/10.5194/essd-13-4529-2021, 2021.

Kuppel, S., Fan, Y., and Jobbágy, E. G.: Seasonal hydrologic buffer on continents: Patterns, drivers and ecological benefits, Advances in Water Resources, 102, 178–187, https://doi.org/10.1016/j.advwatres.2017.01.004, 2017.

Lange, S. and Büchner, M.: ISIMIP2a atmospheric climate input data, https://doi.org/10.48364/ISIMIP.886955, 2020.

Lankford, B., Closas, A., Dalton, J., López Gunn, E., Hess, T., Knox, J. W., van der Kooij, S., Lautze, J., Molden, D., Orr, S., Pittock, J., Richter, B., Riddell, P. J., Scott, C. A., philippe Venot, J., Vos, J., and Zwarteveen, M.: A scale-based framework to understand the promises, pitfalls and paradoxes of irrigation efficiency to meet major water challenges, Global Environmental Change, 65, 102 182, https://doi.org/https://doi.org/10.1016/j.gloenvcha.2020.102182, 2020.

Lendvai, A.: Portale dei dati idrologici italiani, http://meteoniardo.altervista.org/, last access: August 2023, 2020.

Lo Gullo, M. A., Nardini, A., Salleo, S., and Tyree, M. T.: Changes in root hydraulic conductance (KR) of Olea oleaster seedlings following drought stress and irrigation, New Phytologist, 140, 25–31, https://doi.org/10.1046/j.1469-8137.1998.00258.x, 1998.

Lv, G., Kang, Y., Li, L., and Wan, S.: Effect of irrigation methods on root development and profile soil water uptake in winter wheat, Irrigation Science, 28, 387–398, https://doi.org/10.1007/s00271-009-0200-1, 2010.

Maan, C., ten Veldhuis, M.-C., and van de Wiel, B. J. H.: Dynamic root growth in response to depth-varying soil moisture availability: a rhizobox study, Hydrology and Earth System Sciences, 27, 2341–2355, https://doi.org/10.5194/hess-27-2341-2023, 2023.

Martens, B., Miralles, D. G., Lievens, H., Van Der Schalie, R., De Jeu, R. A., Fernández-Prieto, D., Beck, H. E., Dorigo, W. A., and Verhoest, N. E.: GLEAM v3: Satellite-based land evaporation and root-zone soil moisture, Geoscientific Model Development, 10, 1903–1925, https://doi.org/10.5194/gmd-10-1903-2017, 2017.

McCormick, E. L., Dralle, D. N., Hahm, W. J., Tune, A. K., Schmidt, L. M., Chadwick, K. D., and Rempe, D. M.: Widespread woody plant use of water stored in bedrock, Nature, 597, 225–229, https://doi.org/10.1038/s41586-021-03761-3, 2021.

McDermid, S., Nocco, M., Lawston-Parker, P., Keune, J., Pokhrel, Y., Jain, M., Jägermeyr, J., Brocca, L., Massari, C., Jones, A. D., Vahmani, P., Thiery, W., Yao, Y., Bell, A., Chen, L., Dorigo, W., Hanasaki, N., Jasechko, S., Lo, M.-H., Mahmood, R., Mishra, V., Mueller, N. D., Niyogi, D., Rabin, S. S., Sloat, L., Wada, Y., Zappa, L., Chen, F., Cook, B. I., Kim, H., Lombardozzi, D., Polcher, J., Ryu, D., Santanello, J., Satoh, Y., Seneviratne, S., Singh, D., and Yokohata, T.: Irrigation in the Earth system, Nature Reviews Earth & Environment, https://doi.org/10.1038/s43017-023-00438-5, 2023.

Meier, J., Zabel, F., and Mauser, W.: A global approach to estimate irrigated areas - A comparison between different data and statistics, Hydrology and Earth System Sciences, 22, 1119–1133, https://doi.org/10.5194/hess-22-1119-2018, 2018.

Milly, P. C. D.: Climate, soil water storage, and the average annual water balance, Water Resources Research, 30, 2143–2156, https://doi.org/10.1029/94WR00586, 1994.

Miralles, D. G., De Jeu, R. A., Gash, J. H., Holmes, T. R., and Dolman, A. J.: Magnitude and variability of land evaporation and its components at the global scale, Hydrology and Earth System Sciences, 15, 967–981, https://doi.org/10.5194/hess-15-967-2011, 2011.

Miralles, D. G., Brutsaert, W., Dolman, A. J., and Gash, J. H.: On the Use of the Term “Evapotranspiration”, Water Resources Research, 56, e2020WR028 055, https://doi.org/10.1029/2020WR028055, 2020.

Nijzink, R., Hutton, C., Pechlivanidis, I., Capell, R., Arheimer, B., Freer, J., Han, D., Wagener, T., McGuire, K., Savenije, H., and Hrachowitz, M.: The evolution of root-zone moisture capacities after deforestation: a step towards hydrological predictions under change?, Hydrology and Earth System Sciences, 20, 4775–4799, https://doi.org/10.5194/hess-20-4775-2016, 2016.

Roodari, A., Hrachowitz, M., Hassanpour, F., and Yaghoobzadeh, M.: Signatures of human intervention-or not? Downstream intensification of hydrological drought along a large Central Asian river: The individual roles of climate variability and land use change, Hydrology and Earth System Sciences, 25, 1943–1967, https://doi.org/10.5194/hess-25-1943-2021, 2021.

Savenije, H. H.: The importance of interception and why we should delete the term evapotranspiration from our vocabulary, Hydrological processes, 18, 1507–1511, https://doi.org/10.1002/hyp.5563, 2004.

Savenije, H. H. and Hrachowitz, M.: HESS Opinions "catchments as meta-organisms - A new blueprint for hydrological modelling", Hydrology and Earth System Sciences, 21, 1107–1116, https://doi.org/10.5194/hess-21-1107-2017, 2017.

Schlesinger, W. H. and Jasechko, S.: Transpiration in the global water cycle, Agricultural and Forest Meteorology, 189-190, 115 – 117, https://doi.org/10.1016/j.agrformet.2014.01.011, 2014.

Seneviratne, S. I., Corti, T., Davin, E. L., Hirschi, M., Jaeger, E. B., Lehner, I., Orlowsky, B., and Teuling, A. J.: Investigating soil moisture-climate interactions in a changing climate: A review, Earth-Science Reviews, 99, 125–161, https://doi.org/10.1016/j.earscirev.2010.02.004, 2010.

Siebert, S., Burke, J., Faures, J. M., Frenken, K., Hoogeveen, J., Döll, P., and Portmann, F. T.: Groundwater use for irrigation - A global inventory, Hydrology and Earth System Sciences, 14, 1863–1880, https://doi.org/10.5194/hess-14-1863-2010, 2010.

Siebert, S., Kummu, M., Porkka, M., Döll, P., Ramankutty, N., and Scanlon, B. R.: Historical Irrigation Dataset (HID), https://doi.org/doi:/10.13019/M20599, 2015a.

Siebert, S., Kummu, M., Porkka, M., Döll, P., Ramankutty, N., and Scanlon, B. R.: A global data set of the extent of irrigated land from 1900 to 2005, Hydrology and Earth System Sciences, 19, 1521–1545, https://doi.org/10.5194/hess-19-1521-2015, 2015b.

Singh, C., Wang-Erlandsson, L., Fetzer, I., Rockström, J., and Van Der Ent, R.: Rootzone storage capacity reveals drought coping strategies along rainforest-savanna transitions, Environmental Research Letters, 15, https://doi.org/10.1088/1748-9326/abc377, 2020.

Singh, C., van der Ent, R., Wang-Erlandsson, L., and Fetzer, I.: Hydroclimatic adaptation critical to the resilience of tropical forests, Global Change Biology, 28, 2930–2939, https://doi.org/https://doi.org/10.1111/gcb.16115, 2022.

Sivandran, G. and Bras, R. L.: Dynamic root distributions in ecohydrological modeling: A case study at Walnut Gulch Experimental Watershed, Water Resources Research, 49, 3292–3305, https://doi.org/10.1002/wrcr.20245, 2013.

Speich, M. J., Lischke, H., and Zappa, M.: Testing an optimality-based model of rooting zone water storage capacity in temperate forests, Hydrology and Earth System Sciences, 22, 4097–4124, https://doi.org/10.5194/hess-22-4097-2018, 2018.

Stocker, B. D., Tumber-Dávila, S. J., Konings, A. G., Anderson, M. C., Hain, C., and Jackson, R. B.: Global patterns of water storage in the rooting zones of vegetation, Nature geoscience, 16, 250–256, https://doi.org/10.1038/s41561-023-01125-2, 2023.

Van Oorschot, F., Van Der Ent, R. J., Hrachowitz, M., and Alessandri, A.: Climate-controlled root zone parameters show potential to improve water flux simulations by land surface models, Earth System Dynamics, 12, 725–743, https://doi.org/10.5194/esd-12-725-2021, 2021.

Wang, J., Du, G., Tian, J., Zhang, Y., Jiang, C., and Zhang, W.: Effect of irrigation methods on root growth, root-shoot ratio and yield components of cotton by regulating the growth redundancy of root and shoot, Agricultural Water Management, 234, 106 120, https://doi.org/10.1016/j.agwat.2020.106120, 2020.

Wang, K. and Dickinson, R. E.: A review of global terrestrial evapotranspiration: Observation, modeling, climatology, and climatic variability, Reviews of Geophysics, 50, https://doi.org/10.1029/2011RG000373, 2012.

Wang-Erlandsson, L., Bastiaanssen, W. G., Gao, H., Jägermeyr, J., Senay, G. B., Van Dijk, A. I., Guerschman, J. P., Keys, P. W., Gordon, L. J., and Savenije, H. H.: Global root zone storage capacity from satellite-based evaporation, Hydrology and Earth System Sciences, 20, 1459–1481, https://doi.org/10.5194/hess-20-1459-2016, 2016.

Xin, L., Ling, Z., Kun, Z., Donghai, Z., and Gaofeng, Z.: Satellite-based Global Irrigation Water Use data set (2011-2018), https://doi.org/10.11888/Hydro.tpdc.271220, 2021.

Zhang, B., Hautier, Y., Tan, X., You, C., Cadotte, M. W., Chu, C., Jiang, L., Sui, X., Ren, T., Han, X., and Chen, S.: Species responses to changing precipitation depend on trait plasticity rather than trait means and intraspecific variation, Functional Ecology, 34, 2622–2633, https://doi.org/https://doi.org/10.1111/1365-2435.13675, 2020.

570 Zhang, K., Li, X., Zheng, D., Zhang, L., and Zhu, G.: Estimation of Global Irrigation Water Use by the Integration of Multiple Satellite Observations, Water Resources Research, 58, 1–23, https://doi.org/10.1029/2021WR030031, 2022.

Zhao, J., Xu, Z., and Singh, V. P.: Estimation of root zone storage capacity at the catchment scale using improved Mass Curve Technique, Journal of Hydrology, 540, https://doi.org/10.1016/j.jhydrol.2016.07.013, 2016.